RSC Advances

PAPER

View Article Online
View Journal | View Issue

Cite this: *RSC Adv.*, 2019, **9**, 42533

A carbon-rich nanofiber framework based on a conjugated arylacetylene polymer for photocathodic enzymatic bioanalysis†

Junyan Tang,[a] Xiaoya Liu,[a] Chengwei Yang,[a] Zhening Zhang,[a] Rui Sun,[a] Hongmei Li,[a] Caolong Li *[ab] and Fei Wang *[a]

Received 5th November 2019
Accepted 6th December 2019

DOI: 10.1039/c9ra09157b

rsc.li/rsc-advances

Poly(1,3,5-triethynylbenzene) (PTEB), a newly developed conjugated arylacetylene polymer, was utilized for photoelectrochemical (PEC) enzymatic bioanalysis in this work. The porous nanofiber framework of PTEB film which produced an apparent cathodic photocurrent under visible light illumination was fabricated on an indium tin oxide (ITO) electrode *via* copper-surface mediated interface Glaser polycondensation. As the photocurrent density of the metal-free photocathode displayed a characteristic O_2 dependency, the consumption of dissolved oxygen caused by the modified glucose oxidase (GOx) in biocatalysis induced a depressed photoresponse in the presence of glucose. The fabricated PEC transducer exhibited favorable glucose sensing performances in the linear range of 5 μM to 8 mM and with the detection limit of 1.7 μM; it could also be employed in glucose monitoring in human serum. Moreover, the acetylenic carbon-rich polymer possessed the superior features of being cost-effective in preparation and machinable in device development, which sheds light on the exploration of an advanced PEC sensing platform based on conjugated organic polymers for the bioanalysis of valuable analytes.

1. Introduction

Recently, there has been an increasing demand for highly-sensitive and bio-specific analytical methods in areas like health assessment, disease diagnosis, food safety, pharmaceutical analysis and environmental monitoring.[1] Among diverse analytical techniques such as colorimetry, fluorescence, chromatography and electrochemical measures, photoelectrochemical (PEC) bioanalysis is a newly emerging and rapidly developing method.[2,3] Because of the separation of excitation source and detection signal, PEC transducers exhibit higher sensitivity and lower background signals compared with traditional electrochemical sensors.[4,5] Recently, Tang *et al.* reviewed advances in PEC sensing methods from the point of view of rational design and engineering in photoactive materials, sensing devices and detection modes.[6] Moreover, the artful design in PEC systems such as utilizing innovative 'Z-scheme' sensing platforms,[7,8] modifying upconversion nanohybrids[9,10] and regulating optoelectronic characteristics of quantum dots,[11] have made PEC sensing technology become a research hotspot in analytical chemistry over the past few years. Up to now, immunoassay,[12] aptasensors[13,14] and enzymatic biosensors[15] are the three major kinds of PEC transducers. For PEC enzymatic biosensors, the superior sensitivity of PEC analysis and the specific selectivity of enzymes makes the transducer display satisfying sensing performances in various applications.[16]

To date, various PEC sensors have been designed to detect multiple targets through unique sensing mechanisms. The commonly reported PEC transducers are photoanodes which are sensitive to electron donors (*e.g.* ascorbic acid) based on n-type semiconductors. Unlike photoanodes, the photogenerated electrons excited in the conduction band (CB) are prone to interact with electron acceptors (*e.g.* dissolved oxygen) on the surface of photocathodes, which will improve the anti-interference capability against reductive substances, especially when analyzing real biological samples.[15,17] On the other hand, the photogenerated holes will accept the electrons from the counter electrode so that the photocathode can to a large extent avoid self-oxidation and show better stability in PEC tests.[18] Compared with the anodic PEC sensing mode, cathodic PEC transducers display more superiority in bioanalysis. Therefore, it is indispensable to develop innovative photocathodes based on p-type semiconductors for PEC bioanalysis.

Throughout semiconductors, the prevalent photocatalytic materials such as TiO_2,[19,20] ZnO,[21] Fe_2O_3,[22,23] CdS,[24–26] CuS,[27] MoS_2 (ref. 5, 28 and 29) and graphitic carbon nitride (g-C_3N_4)[30,31] have been used to construct photoelectrodes for PEC analysis. However, the above listed materials suffered from quite a few

[a]*Key Laboratory of Biomedical Functional Materials, School of Science, China Pharmaceutical University, Nanjing, 211198, P. R. China. E-mail: feiwang@cpu.edu.cn; licl@cpu.edu.cn*

[b]*Tibetan Medicine Research Institute, Tibetan Traditional Medical College, Tibet, 850000, P. R. China*

† Electronic supplementary information (ESI) available. See DOI: 10.1039/c9ra09157b

drawbacks such as poor response in the visible spectrum, rapid recombination of photogenerated electron–hole pairs, low specific surface areas as well as photocorrosion effects.[18,30] Despite enhanced photoresponse by constructing hetero-junctions,[32–34] doping hetero-atoms[30] and modifying noble metals,[27,35] the inherent defects of anodic PEC bioanalysis still limit the wide utilization of these materials in this field. To design more satisfying PEC transducers, it is highly attractive and challengeable to pursue novel photoactive materials for cathodic PEC bioanalysis.

Recently, a series of active metal-free photocathodes based on conjugated arylacetylene polymer (CAP) have been utilized in PEC water reduction.[36–38] The extended π-conjugation structure formed through the diacetylenic linkages between each monomer bestows the unique optical, electronic and mechanical properties to these 2D-polymers. As a representative CAP constructed by the homo-coupling of C_3 symmetric building block, poly(1,3,5-triethynylbenzene) (PTEB) showed proper absorption in visible spectrum and suitable band energy edge position for photocatalytic water splitting. The PTEB nanosheets synthesized by Xu *et al.* could act as an efficient photocatalyst for overall water splitting under visible light without using sacrificial reagents.[39] Besides, the p-type semiconductor PEC behavior of PTEB indicated its excellent usage for cathodic PEC bioanalysis.[36] Compared with the metal-based p-type semiconductors such as Cu_2O,[40,41] NiO,[42] BiOI,[43,44] $CuBi_2O_4$ (ref. 17) and $CuInS_2$,[15] PTEB manifested apparent photocurrent response and outstanding stability in PEC test. Furthermore, the naturally abundant element source of carbon is beneficial for the large-scale application of the metal-free acetylenic polymer in comparison with rare metal.

In our study, porous PTEB nanofiber film was synthesized on indium tin oxide (ITO) electrode *via* copper-surface mediated interface Glaser polycondensation (Scheme 1a). As the PTEB photocathode is specifically sensitive to O_2, the positive correlationship in cathodic photocurrent density *versus* the content of dissolve oxygen in electrolyte can be adapted for indirect PEC analysis. In light of the fact that the competition of O_2 consumption between the enzyme biocatalytic reaction and the reduction of O_2 on photocathodes has been widely utilized to construct PEC enzymatic biosensor,[45] the modified glucose oxidase (GOx) on PTEB photocathode realized the "signal off" sensing of glucose on the bias of the depressed photocurrent and the designed PEC sensor was successfully applied to detect glucose level in human serum samples. The visible light response of PTEB could maintain the enzyme activity and improve the operation safety of the PEC transducer. In addition, the *in situ* formed nanofiber film on arbitrary substrate exhibited promising machinability in device development. This work suggests that conjugated organic polymer with well PEC performance are worth further investigating in PEC bioanalysis.

2. Experimental section

2.1 Materials and reagents

1,3,5-Triethynylbenzene (TEB) and glucose oxidase (10 000 GODU per g) were purchased from Energy Chemical Technology (Shanghai) Co., Ltd. and Shanghai Yuanye Biotechnology Co., Ltd., respectively. Copper foil, D-(−)-fructose, D-(+)-mannose, D-(+)-galactose, L-arginine (L-Arg), L-lysine (L-Lys), dopamine, acetaminophen and poly-(diallyldimethylammonium chloride) (PDDA, 20 wt% in water, M_W = 200 000–350 000) were obtained from Shanghai Aladdin Biochemical Technology Co., Ltd. D-(+)-Glucose, ascorbic acid (AA), L-glycine (L-Gly), maltose, sucrose, piperidine, dichloromethane, methanol, acetone, ethanol, NaCl, KCl, NaH_2PO_4 and Na_2HPO_4 were acquired from Sinopharm Chemical Reagent Co., Ltd. Pyridine, hydrochloric acid and H_2O_2 were obtained from Nanjing Chemical Reagent Co., Ltd. The indium tin oxide (ITO) glass (10 × 20 × 1.1 mm with an ITO film of 185 ± 2 nm and a sheet resistance of 6.6 ± 0.1 Ω) was supplied from Shenzhen South Xiangcheng Technology Co., Ltd. Human serum samples were collected from Sir Run Run Hospital, Nanjing Medical University. Deionized water was used in all experiments.

2.2 Apparatus

The morphology and microstructure of PTEB film were characterized by HITACHI SU800 scanning electron microscopy (SEM) and Tecnai G2 F20 transmission electron microscopy (TEM), respectively. Ultraviolet-visible (UV-vis) spectrum was obtained on Hitachi U3900 spectrophotometer. Fourier-transform infrared spectra (FT-IR) and Raman spectra were analyzed by Shimadzu IRAffinity-1S spectrometer and Renishaw inVia plus spectroscope (with excitation laser wavelength at 514 nm), respectively. X-ray photoelectron spectroscopy (XPS) spectra were collected on Thermo ESCALAB 250XI spectrometer. All PEC tests were performed on CHI 660E electrochemical workstation. A 500 W xenon lamp equipped with a 420 nm cutoff filter was employed as the irradiation source and the light intensity was controlled at 80 mW cm^{-2} by the photometer in PEC tests.

2.3 Synthesis PTEB nanofiber film on ITO substrate *via* interface polymerization

Firstly, the ITO substrate (1 cm × 2 cm) was cleaned by acetone, ethanol and deionized water, respectively under sonication, and then dried by argon flow. The copper foil (1 cm × 2 cm) was pretreated in 3 M HCl to remove the peripheral oxides and hydroxides. Then, the ITO conductive surface was covered by copper foil and were transferred into the reaction flask immediately. The concentration of TEB monomer and piperidine ligand in pyridine solvent were controlled at 0.5 mg mL^{-1} and 1 μL mL^{-1}, respectively. Afterwards, the above reaction agents were added into the flask carefully and the reaction was held in a 60 °C oven for 24 h. After reaction, the ITO electrode and copper foil were washed with fresh pyridine, dichloromethane and methanol successively. Finally, the substrate was dried under a flow of argon and the golden PTEB film was uniformly coated on the ITO surface. Besides, we also prepared bulk PTEB in aggregated sheet shape for comparing the PEC performances of PTEB in various microstructure and the detailed synthesis procedures of bulk PTEB were listed in ESI.†

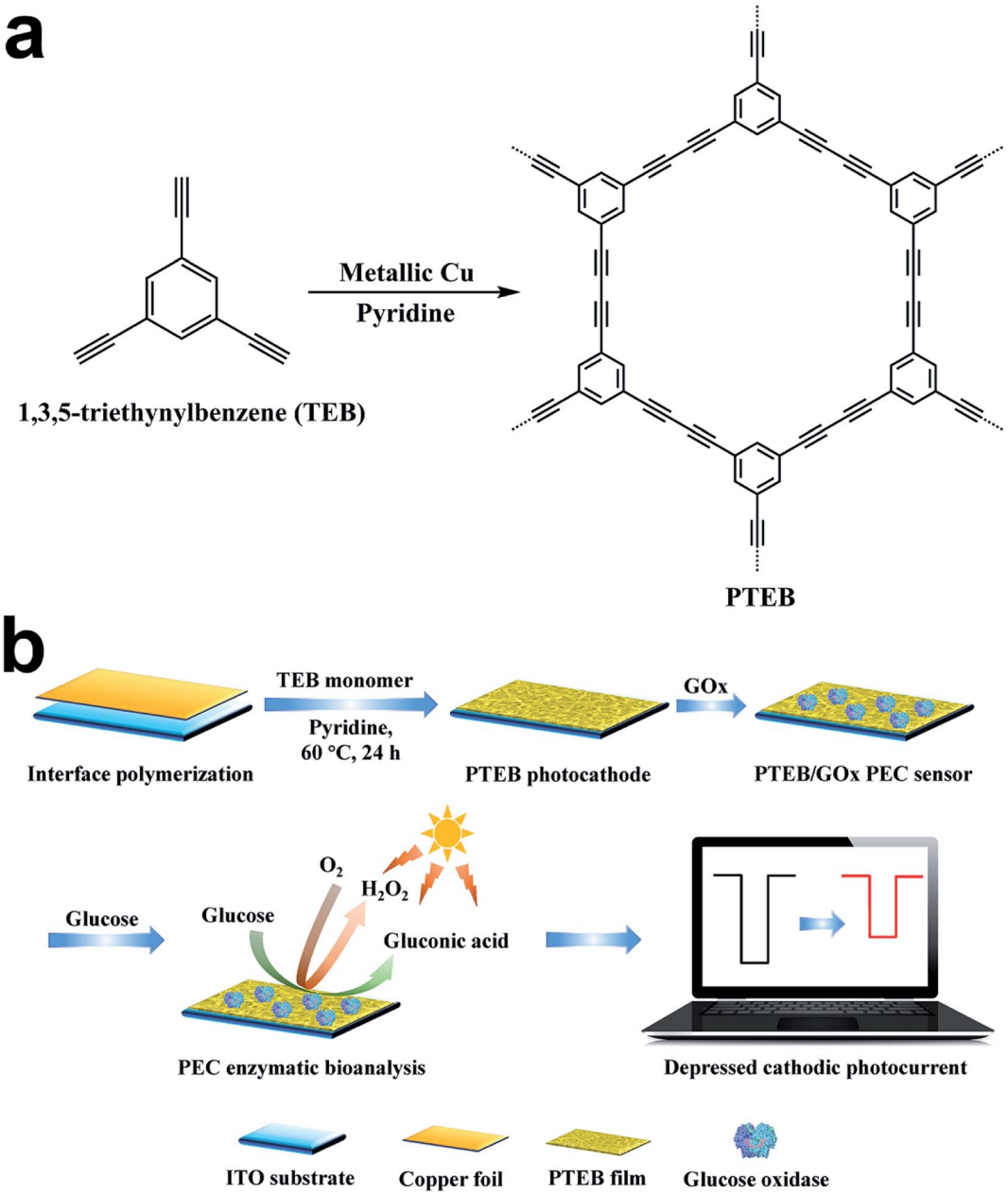

Scheme 1 (a) Chemical structures of TEB and PTEB. (b) Synthesis of PTEB nanofiber film on ITO substrate *via* interface polymerization and fabrication process of PEC glucose sensor based on glucose oxidase.

2.4 Fabrication of PEC glucose sensor based on GOx

In order to immobilize glucose oxidase more firmly on the surface of PTEB photocathode, we dropped 25 μL 2 wt% PDDA containing 0.5 M NaCl on the fabricated photoelectrode. 1 h later, the electrode was rinsed with ultrapure water and then 25 μL 5.0 mg mL^{-1} GOx was drop-casted. The electrode was incubated for another 1 h at room temperature and then washed by ultrapure water again to remove the uncombined enzyme. Finally, the GOx modified PTEB photocathode was stored at 4 °C before PEC test. The entire preparation process of the PEC glucose sensor is illustrated in Scheme 1b.

2.5 PEC measurements

PEC measurements were performed in the three electrodes cell consisting of PTEB photocathode as the working electrode, Pt wire and Ag/AgCl as the counter electrode and reference electrode, respectively. The air-saturated 0.1 M pH 7.0 phosphate buffer solution (PBS) was used as the electrolyte in PEC tests at room temperature. The photocurrent density was calculated based on the irradiated surface area of 1.0 cm^2 of the photocathode. To determine the glucose level in human serum samples, 200 μL serum sample was added into 20 mL PBS for PEC bioanalysis and the obtained results from the transducer were compared with that measured by the hospital.

2.6 Live subject statement

The authors state that all experiments were performed in compliance with the relevant laws and institutional guidelines. The institutional committee of the Sir Run Run Hospital, Nanjing Medical University approved the experiment. The authors also state that informed consent was obtained for any experimentation with human subjects and the human serum samples used in this study didn't have any identifying information about all the participants that provided written informed consent. The Sir Run Run Hospital, Nanjing Medical University is committed to the protection and safety of human subjects involved in the research.

3. Results and discussion

3.1 Characterization of PTEB nanofiber film on ITO substrate

The copper foil utilized in the preparation of PTEB film was the source of catalyst for Glaser coupling reaction. The catalytic copper species such as Cu^{I} and Cu^{II} were generated from the surface of copper foil and further diffused into the interface monomer solution. The solubilized copper species would catalyze the coupling reaction of TEB; the PTEB film would gradually *in situ* form on the ITO substrate. From the top view of SEM images in Fig. 1a and b, the acetylenic framework is composed of tiny nanofibers and the diameter of each individual nanofiber ranges from 10 to 20 nm. Some nanofibers tend to adhere together and form larger bundles, and they are connected to form porous mesh microstructure in TEM image (Fig. 1d). After the polycondensation reaction, the thickness of the PTEB nanofiber film is determined to be 430 nm from the cross-section view in Fig. 1c.

PTEB film shows proper absorption in visible region with an absorption edge of 520 nm in its UV-vis absorption spectrum (Fig. 2a), which is in accordance with the golden appearance of the photoelectrode (lower-left inset in Fig. 2a). According to the analysis of Tauc plot, the calculated direct optical bandgap of PTEB is 2.40 eV (upper-right inset in Fig. 2a). The narrower bandgap compared with g-C_3N_4 nanosheets (2.7 eV)[30,46] indicates PTEB would possess higher utilization efficiency of visible light as an innovative metal-free photoactive material. The optical properties of PTEB demonstrate that this polymer is suitable for high performance PEC bioanalysis. The structure of PTEB is confirmed by the infrared spectroscopy. The typical peaks attributed to alkyne and aromatic ring are labeled in Fig. 2b. Comparing the vibration peak position of –C≡C– between TEB monomer and PTEB film, the blue shift of the peak located at 2111 cm^{-1} to 2213 cm^{-1} reflects the formation of diacetylenic in PTEB framework. The similar peaks can be observed in the FT-IR spectrum of bulk PTEB (Fig. S1a†), which stresses the successful preparation of PTEB in various microscopic morphology *via* two different methods.

The chemical composition of the PTEB film covered on ITO substrate is further examined by XPS. Except the existence of In, Sn and O elements which are originated from In_2O_3 and SnO_2 in the ITO layer, the XPS survey spectrum in Fig. 2c reveals that the PTEB film only contains elemental carbon. The divided two peaks at 284.6 eV and 285.3 eV in C 1s high-resolution XPS spectrum (Fig. 2d) are corresponding to sp^2 and sp hybridized carbons, respectively.[39] In addition, the broad neighboring peak

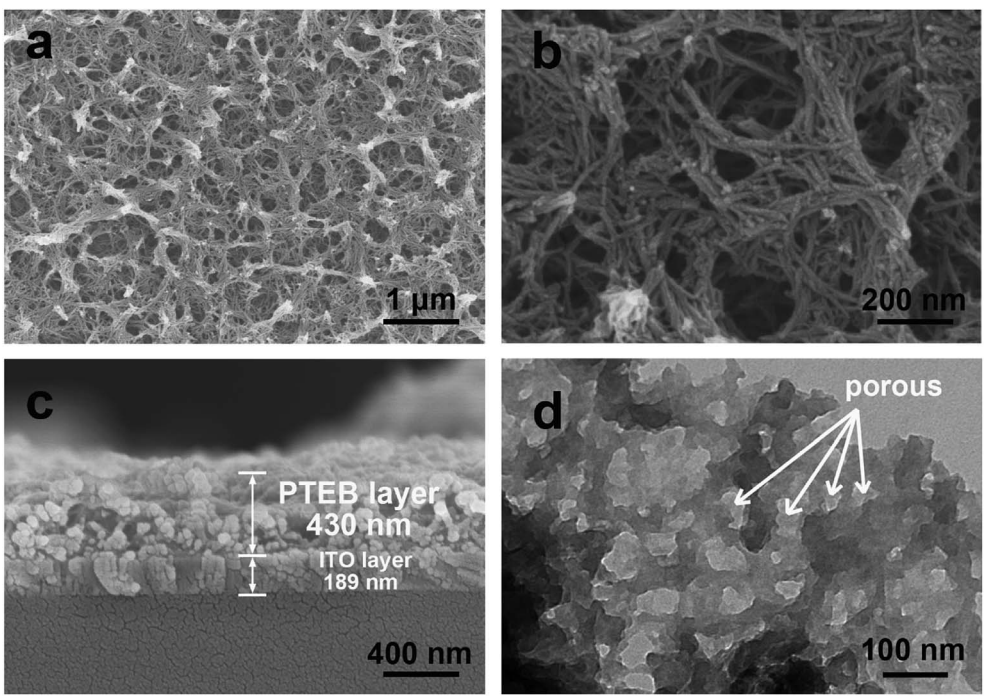

Fig. 1 Morphology and microstructure characterization of PTEB nanofiber film. (a) Top view and (b) magnified SEM images of PTEB nanofiber film. (c) Cross-section view of SEM image of PTEB film coated on ITO electrode. (d) TEM image of PTEB framework exfoliated from the ITO substrate.

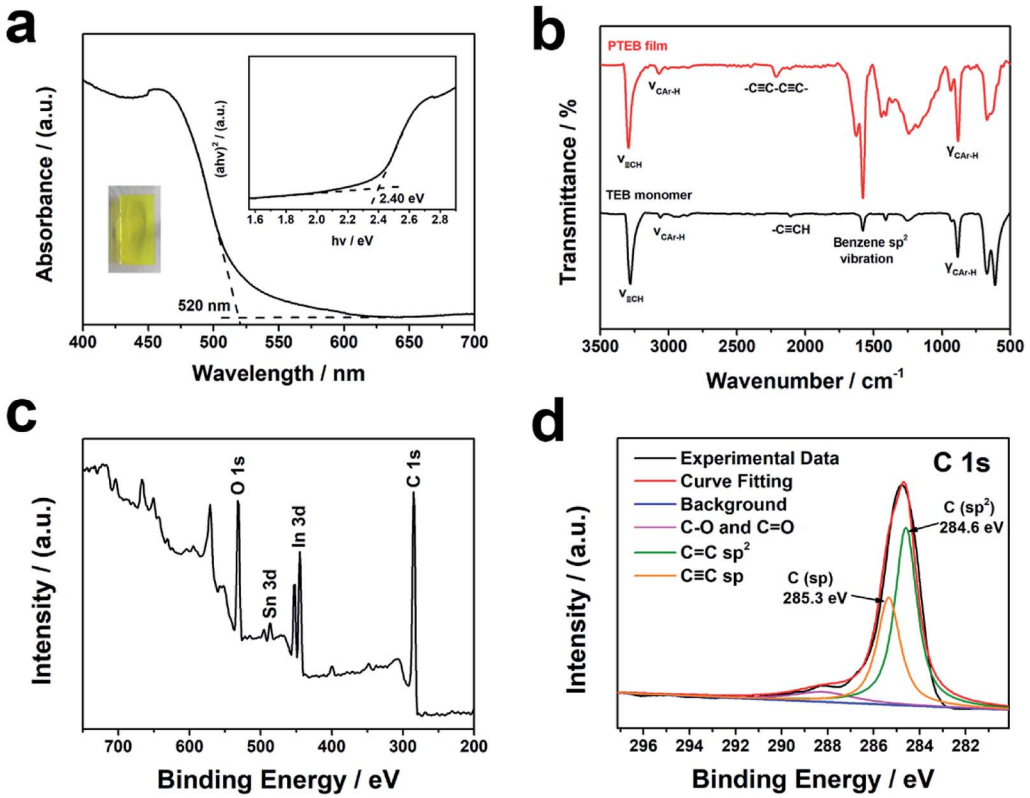

Fig. 2 Optical properties and chemical composition of PTEB photoelectrode. (a) UV-vis absorption spectrum of PTEB film covered on ITO electrode. Inset: the digital photograph and the $(\alpha h\nu)^2$ *vs.* $h\nu$ curve of PTEB film. (b) FT-IR spectra of TEB monomer (black) and PTEB film (red). XPS survey spectrum (c) and C 1s high-resolution XPS spectrum (d) of PTEB film on ITO substrate.

with weak intensity is related with the C–O and C═O bond, which could be ascribed to the small oxygenated substances (*e.g.* H_2O, O_2, CO_2) adsorbed in the porous PTEB nanofiber framework.

3.2 Photoelectrochemical characterization of the PTEB photocathode

As the charge carriers in semiconductor acquire the photon energy under irradiation, the separation and migration of electro–hole pairs will lead to the generation of photocurrent, which aligns with the significant photoresponse in the linear sweep voltammetry (LSV) curve of PTEB film (Fig. S2†). The photocurrent densities of bare ITO substrate and PTEB modified photoelectrodes are shown in Fig. 3a. No photocurrent response was observed on bare ITO substrate under light illumination, but the PTEB modified photoelectrodes made prompt and apparent photocurrent response to the on–off illumination cycles, as a result of favorable optical properties of PTEB in visible spectrum. The appearance of cathodic photocurrent under the applied negative potential (*vs.* Ag/AgCl) demonstrated that PTEB accorded with the PEC features of p-type semiconductor.[47] Furthermore, the photocathode based on PTEB film produced much stronger photocurrent and the charge transfer resistance of PTEB film was reduced obviously under illumination in the Nyquist plot (Fig. 3b) compared with bulk PTEB (Fig. S3†). These results recognized the depressed recombination of electron–hole pairs and the prolonged lifetime of photogenerated carriers in PTEB film. By analyzing the discrepancy in the microstructure between the nanofiber framework of PTEB film and the aggregated sheet morphology of bulk PTEB (Fig. S1b†), we inferred that the photogenerated electron could transfer through the nanofibers to the surface of PTEB film and then react with the electron accepter in electrolyte to yield higher photocurrent response. However, the charge carriers might recombine swiftly in the stacked layer of bulk PTEB, which would inhibit the reductive reaction on the photoelectrode–electrolyte interface. The difference in the intensity of photocurrent demonstrated that the nanofiber framework was beneficial for promoting the PEC performance of PTEB as an outstanding visible light sensitive material for cathodic PEC bioanalysis.

As for obtaining the ideal photocurrent response, the effect of bias potential on the photocurrent density of PTEB photocathode was studied to clarify the influence on the recombination probability of the electron–hole pairs.[48] The photocurrent response of PTEB film and the corresponding plot at the potentials from 0 to −0.5 V are shown in Fig. 3c and S4,† respectively. As a p-type semiconductor, PTEB film exhibited increased photocurrent response when the negative bias was applied because the negative potential was helpful to the separation and migration of electrons and holes.[48] The generated photocurrent density reached maximum of 30 μA cm^{-2} at

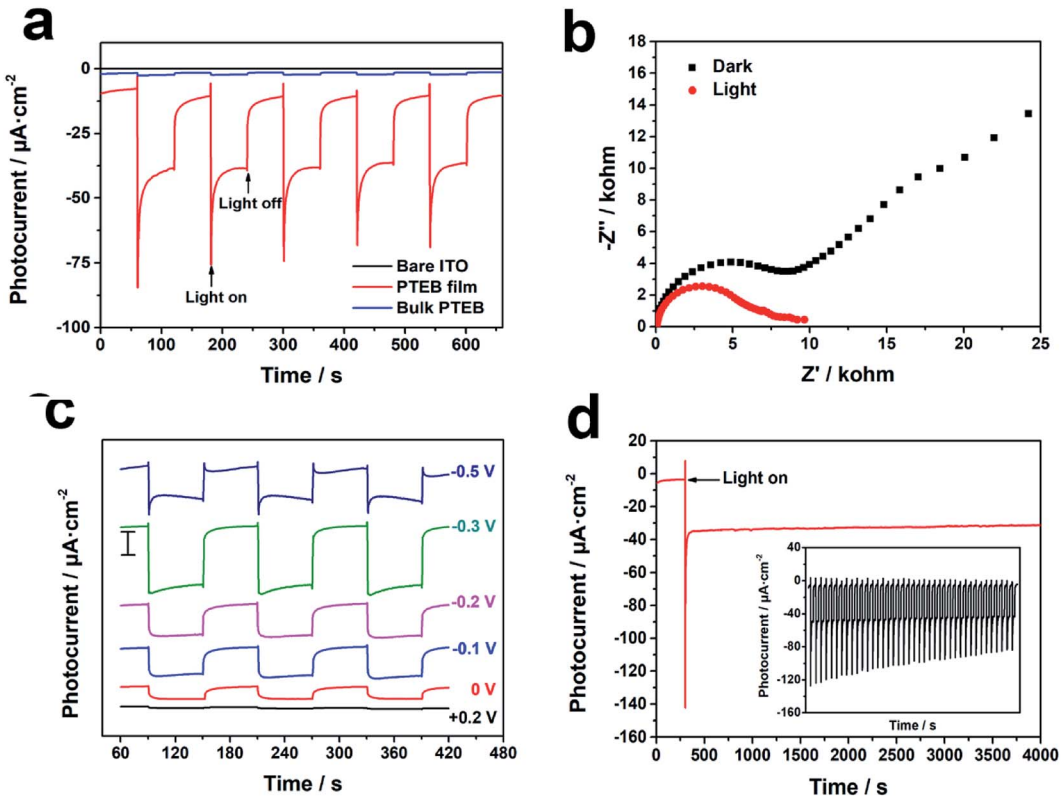

Fig. 3 PEC characterization of the PTEB photocathode. (a) Photocurrent density *vs.* time at −0.3 V *vs.* Ag/AgCl of ITO substrate (black), PTEB film (red) and bulk PTEB (blue) under intermittent irradiation ($\lambda \geq 420$ nm, 80 mW cm^{-2}). (b) Nyquist plots of PTEB film under dark and illumination (bias: −0.3 V *vs.* Ag/AgCl, amplitude: 5 mV, frequency range: 100 kHz to 0.01 Hz). (c) The effect of bias potential (from 0.2 V to −0.5 V *vs.* Ag/AgCl) on the photocurrent response of PTEB photocathode, scale bar: ~15 μA cm^{-2}. (d) Photocurrent density of the PTEB photocathode under 1 h continuous illumination and the photoresponse stability test by repeated on–off irradiation cycles (inset).

−0.3 V. However, the photocurrent density decreased when the applied potential was lower than −0.5 V and the signal was unstable. Considering the amplified photoresponse and the stable signal simultaneously, −0.3 V *vs.* Ag/AgCl was chosen as the optimal bias potential in the further PEC tests.

The stability of the PTEB photocathode under light irradiation is another key factor to be estimated. After 1 h of continuous illumination, the photocurrent of the photocathode showed insignificant decrease and the current density maintained 93% of the initial value which remained at the start of irradiation (Fig. 3d). The inset in Fig. 3d showed that the photocathode displayed reproducible photocurrent response in 40 repeated on–off illumination cycles. Besides, Raman spectroscopy was utilized to investigate the structural stability of PTEB in PEC test (Fig. S5†). The sharp peak at 2219 cm^{-1} is the characteristic vibration mode of 1,3-diacetylenic linkage and the peaks at 993 cm^{-1}, 1343 cm^{-1}, 1584 cm^{-1} are assigned to the breathing and stretching of aromatic rings.[49,50] The unchanged Raman spectrum of PTEB film after irradiation demonstrated that the favorable structural stability of PTEB. Moreover, the SEM images in Fig. S6† showed that the morphology of PTEB nanofiber framework on ITO substrate maintained well after continuous illumination, suggesting the outstanding photophysical stability of PTEB photocathode.

3.3 Photoelectrochemical determination of glucose based on PTEB photocathode

Glucose oxidase was immobilized on the surface of photoelectrode effectively *via* the electrostatic interaction between the positive PDDA layer and the negative enzyme.[43] The electron transfer resistance (R_{et}) rose after the photoelectrode was incubated with enzyme suspension, resulting from the formation of charge barrier layer induced by biomacromolecule.[51] The transform of R_{et} in Fig. S7† confirmed that the GOx was successfully combined on the photoelectrode. Fig. 4a and b demonstrated that the cathodic photocurrent density depressed steadily with the increase of glucose concentration. ΔI represented the photocurrent response in the presence of glucose subtracted by the dark current. The value of ΔI displayed a good linear relationship with the logarithm of glucose concentration from 5 μM to 8 mM in the inset of Fig. 4b and the regression equation was $\Delta I\,(\mu A\ cm^{-2}) = 3.55\ \log C_{glucose}\,(\mu M) - 38.29$ ($R^2 = 0.995$). The detection limit (LOD) of the PEC glucose sensor was calculated of 1.7 μM by the equation of LOD $= tS/M$, where t is the parallel determination times of the blank sample; S and M are the standard deviation of the background current and the sensitivity of the sensor, respectively. As a newly developed conjugated arylacetylene polymer, the photocathode based on

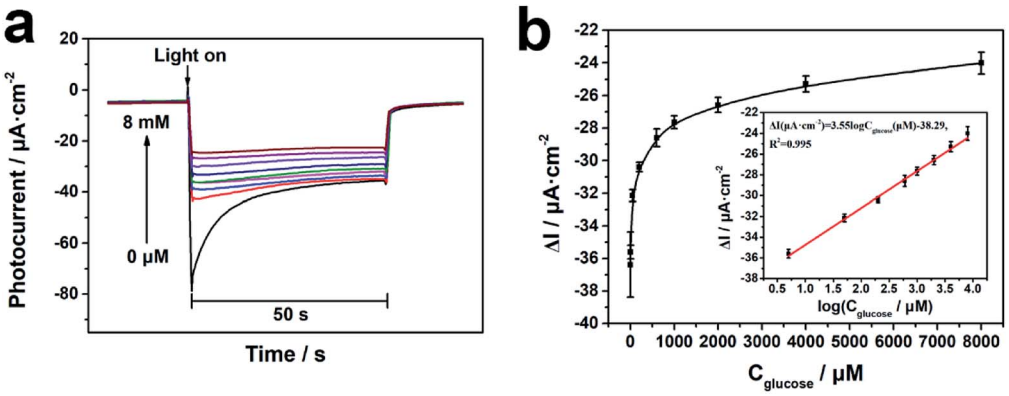

Fig. 4 PEC measurements of glucose by the PTEB photocathode. (a) The depressed photocurrent responses of the GOx modified PTEB photocathode at the applied bias of −0.3 V with the increasing glucose concentration in air-saturated 0.1 M PBS (pH 7.0). (b) The corresponding plot of Δ*I vs.* glucose concentration from 5 μM to 8 mM and the calibration curve based on the calculation results (inset).

PTEB showed preferable analytical performance with other PEC glucose sensors listed in Table S1† and the visible light response property was beneficial for retaining the bioactivity of enzyme in a long time. It should be also noticed that a large number of photoactive materials in PEC glucose sensor belong to n-type semiconductor and the photoanodes based on n-type semiconductor are prone to interact with electron donors in the electrolyte. As real biological samples usually contain various reductive agents, the intrinsic hole oxidation may induce the unreal signal response in the sensing system, which limits the application of photoanodes in PEC bioanalysis. Therefore, the p-type semiconductor feature of PTEB which is favorable for cathodic PEC biosensing is the main advantage compared with the previously reported photoactive materials. Moreover, PTEB and other photoactive conjugated organic polymer may provide more choices in the selection of metal-free material utilized in PEC bioanalysis.

Selectivity, repeatability, stability and reproducibility were further investigated to estimate the sensing performance of the PEC transducer. The PTEB photocathode displayed good anti-interference to the glucose analogues, which was contributed by the specific catalysis of enzyme (Fig. 5a). In addition, some inorganic salts, amino acids and reductive biomolecules commonly existed in human fluid showed insignificant influence on the response of glucose (Fig. 5b), which revealed the satisfied selectivity of PTEB photocathode for PEC enzymatic glucose bioanalysis. The result of the repeatability test in Fig. 5c showed that the photocurrent response was quite stable in the presence of 1 mM glucose under 10 repeated on/off illumination cycles and the relative standard deviation (RSD) was calculated to be 0.81%. After seven days storage at 4 °C, the photoelectrode remained 95.6% of the initial current response which implied the promising long-term stability of the PEC sensor. For reproducibility assessment, six individual photoelectrode were prepared and the RSD of the responses in detection of 1 mM glucose was 2.7%, suggesting the good reproducibility of the transducer.

3.4 Sensing mechanism of the cathodic PEC bioanalysis

The PEC properties of PTEB manifested its characteristic of p-type semiconductor. According to the migration direction of charge carriers, the electron accepter would be easily reduced by the stimulated photogenerated electron. In this regard, we firstly analyzed the effect of Cu^{2+}, a typical electron scavenger, on the photocurrent density of PTEB film in deoxygenated electrolyte. The amplified photocurrent with the increasing concentration of Cu^{2+} was observed in Fig. S8,† resulting from the inhibited recombination of the electron–hole pairs caused by Cu^{2+} reduction.[52] Considering that dissolved oxygen is the common existed electron accepter in electrolyte, the "signal off" sensing feature in PEC measurements of glucose suggests that the consumption of dissolved oxygen by the GOx biocatalysis reaction is associated with the sensing mechanism of the PEC transducer. In order to validate the possible mechanism, we investigated the relationship between the photocurrent density and the content of dissolved oxygen in electrolyte. As shown in Fig. 5d, the deoxygenation operation of argon purging (red) or the addition of Na_2SO_3, O_2 scavenger (blue), would inhibit the cathodic photocurrent response effectively. Besides, H_2O_2, another possible electron accepter in the electrolyte produced from bioconversion,[42,43] exerted no obvious influence on the photocurrent density (Fig. S9†), implying the photocathode was more sensitive to the dissolved oxygen as the main electron accepter in this biosensing system. On the other hand, the value of highest occupied molecular orbital (HOMO) and lowest unoccupied molecular orbital (LUMO) levels of PTEB nanofiber were calculated to be 1.83 V and −0.68 V (*vs.* NHE), respectively in the previous report.[36] As the LUMO level was more negative than the reduction potential of dissolved oxygen $E^{\theta}(O_2/O_2^{-\bullet}) = -0.33$ V (*vs.* NHE),[53,54] the photogenerated electron in LUMO could be captured by the dissolved oxygen as electron accepter in air-saturated electrolyte, which was accord with experiment results showed in Fig. 5d. The band structure diagram of PTEB nanofiber and the charge transfer process under light illumination were described detailly in Fig. S10.† Thus, the sensing principle of the developed PEC sensor could be illustrated

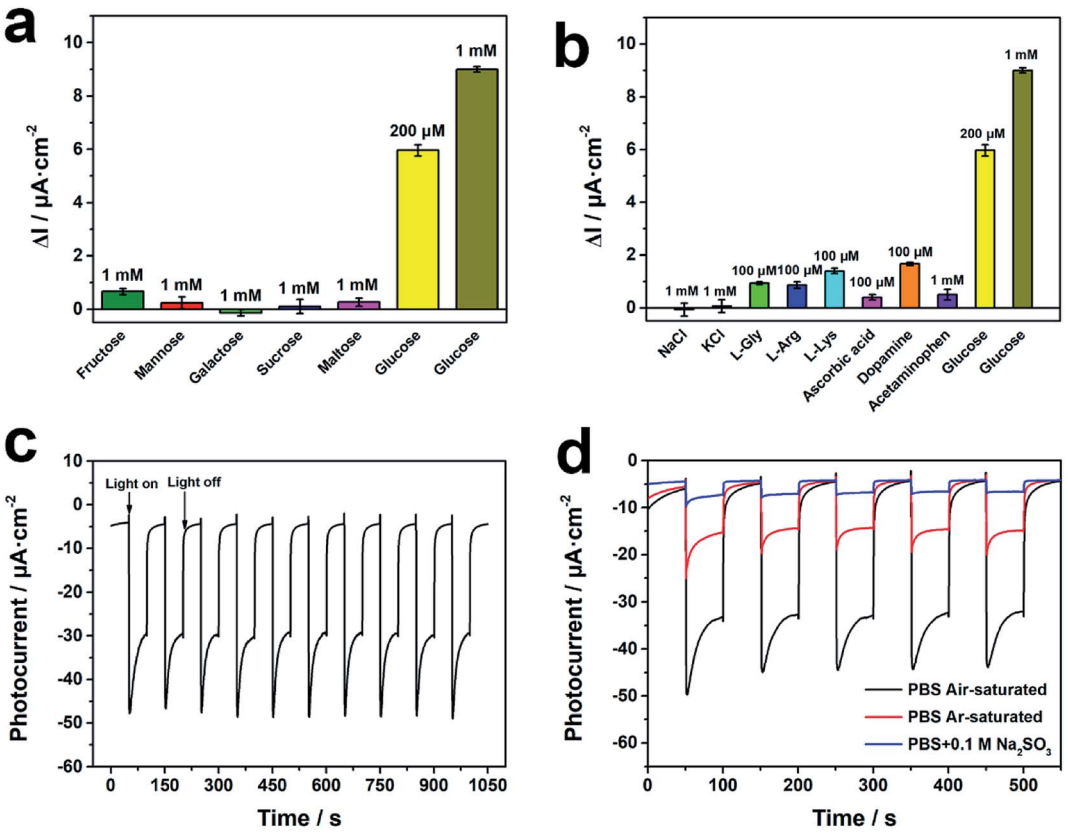

Fig. 5 Evaluation of sensing performances and mechanism research of the PEC sensor. Effect of (a) glucose analogues, (b) inorganic salts, amino acids and reductive biomolecules on the photocurrent response compared with glucose. The error bars represent the standard deviation of five parallel measurements. (c) Photocurrent response of the PTEB photocathode in the presence of 1 mM glucose under 10 repeated on/off illumination cycles. (d) Photocurrent responses of PTEB photocathode in air-saturated (black), Ar-saturated (red), Na_2SO_3 added 0.1 M PBS (pH 7.0).

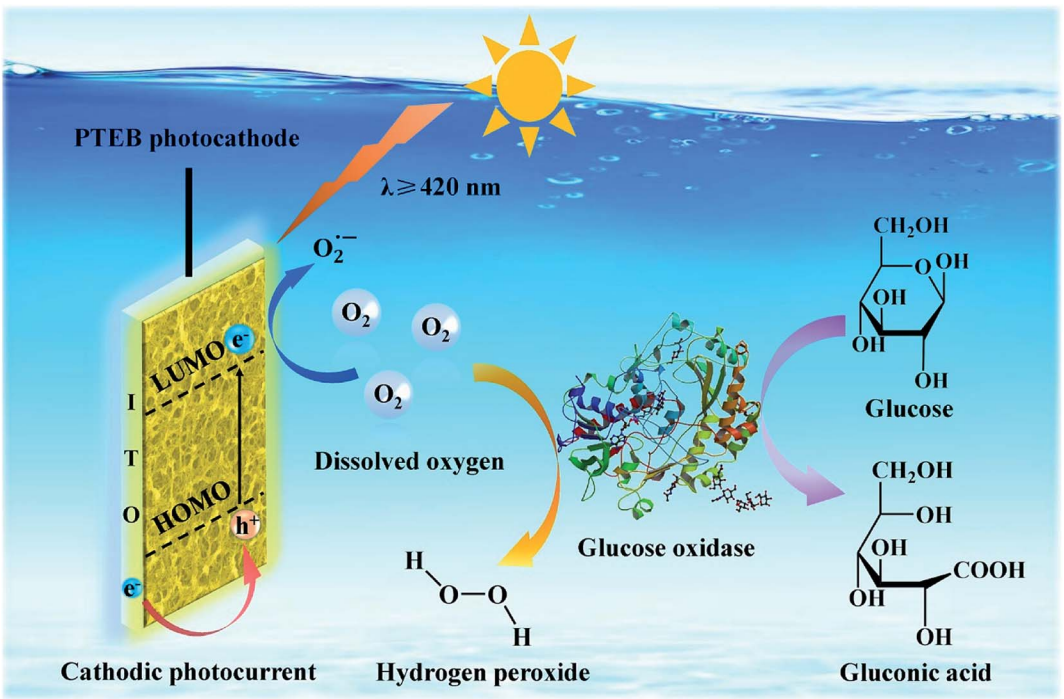

Scheme 2 Proposed sensing mechanism of the PEC enzymatic glucose transducer based on PTEB photocathode.

Table 1 Determination of glucose level in human serum samples

Sample	Measurement value from the hospital (mM)	Concentration detected by the PEC sensor (mM)	RE (%)	RSD (%) ($n = 5$)
1	4.63	4.68	1.1	4.9
2	5.72	5.48	−4.4	3.3
3	9.54	9.52	−0.2	5.7

briefly in Scheme 2. As an O_2-dependent photocathode, the dissolved oxygen would diffuse on the photoelectrode surface and capture the photogenerated electron from the LUMO in PTEB under light illumination. When glucose was spiked into the electrolyte, the dissolved oxygen would be reduced to H_2O_2 simultaneously during the enzymatic conversion of glucose to gluconic acid. The quantitative consumption of dissolved oxygen would further induce the decrease of cathodic photocurrent and the relationship between the inhibition of photocurrent density and glucose concentration could be utilized in the indirect PEC enzymatic bioanalysis of glucose.

3.5 Analysis of glucose in human serum samples

To evaluate the capability of glucose monitoring in complex biological fluid for potential application, we further used the PTEB photocathode to detect glucose level in real human serum samples. The serum samples were diluted 100 times by 0.1 M PBS (pH 7.0) and the depressed cathodic photocurrent could be observed in the presence of serum samples (Fig. S11†). The measurement results are shown in Table 1. The relative error (RE) and relative standard deviation (RSD) were calculated within 6.0%, which implied that the measured results by PEC sensor were in good agreement with the values from hospital. The favorable sensing accuracy and reliability suggested the promising applicability of the PTEB photocathode for practical utilization in PEC bioanalysis of real sample.

4. Conclusion

In summary, an innovative PTEB photocathode was constructed *via* copper-surface mediated interface polymerization in this work for cathodic PEC enzymatic bioanalysis. The porous nanofiber framework of PTEB film displayed preferable PEC performances against the aggregated bulk PTEB due to the facilitated separation and migration of charge carriers. As an O_2-dependent photocathode, the modification of GOx realized "signal off" glucose monitoring with favorable sensing performances. The successful determination of glucose level in human serum also suggested the potential application of the sensor in diabetes diagnosis. Meanwhile, the visible light response of PTEB ensured the preservation of enzyme activity and the operation safety of the PEC transducer. Moreover, the metal-free conjugated polymer possessed more advantages such as being cost-effective in preparation, high biocompatibility in live bioassay and promising machinability in device development. In the future, the PEC performance of conjugated acetylenic polymer could be promoted *via* molecular engineering strategy and the artful designed sensing principle could be utilized to exploit more advanced PEC sensors for bioanalysis of interesting targets.

Conflicts of interest

There are no conflicts of interest to declare.

Acknowledgements

We appreciate the financial support by the National Natural Science Foundation of China (81660708), Natural Science Foundation of Jiangsu Province of China (BK20171389), Science and Technology Support Program of Jiangsu Province (BE2018389) and the Key Project of Tibetan Medical Administration of Tibet (2017005). The work is also supported by "Double First-Class" University Project (CPU2018GY25), the Qinglan Project of Young Academic Leaders of Jiangsu Province, Fundamental Research Funds for the Central Universities (2632019YX01) and Postgraduate Research & Practice Innovation Program of Jiangsu Province (KYCX19_0622).

References

1 R. Gill, M. Zayats and I. Willner, *Angew. Chem., Int. Ed. Engl.*, 2008, **47**, 7602–7625.
2 J. Tang, Y. C. Wang, J. Li, P. M. Da, J. Geng and G. F. Zheng, *J. Mater. Chem. A*, 2014, **2**, 6153–6157.
3 Z. Yue, F. Lisdat, W. J. Parak, S. G. Hickey, L. P. Tu, N. Sabir, D. Dorfs and N. C. Bigall, *ACS Appl. Mater. Interfaces*, 2013, **5**, 2800–2814.
4 X. R. Zhang, Y. S. Guo, M. S. Liu and S. S. Zhang, *RSC Adv.*, 2013, **3**, 2846–2857.
5 S. Y. Wu, H. Huang, M. X. Shang, C. C. Du, Y. Wu and W. B. Song, *Biosens. Bioelectron.*, 2017, **92**, 646–653.
6 J. Shu and D. Tang, *Anal. Chem.*, 2019, DOI: 10.1021/acs.analchem.9b04199.
7 S. Z. Lv, K. Y. Zhang, Y. Y. Zeng and D. P. Tang, *Anal. Chem.*, 2018, **90**, 7086–7093.
8 R. J. Zeng, Z. B. Luo, L. S. Su, L. J. Zhang, D. P. Tang, R. Niessner and D. Knopp, *Anal. Chem.*, 2019, **91**, 2447–2454.
9 Z. L. Qiu, J. Shu, J. F. Liu and D. P. Tang, *Anal. Chem.*, 2019, **91**, 1260–1268.
10 Z. B. Luo, Q. G. Qi, L. J. Zhang, R. J. Zeng, L. S. Su and D. P. Tang, *Anal. Chem.*, 2019, **91**, 4149–4156.
11 J. Shu and D. P. Tang, *Chem.–Asian J.*, 2017, **12**, 2780–2789.

12 S. Lv, K. Y. Zhang, Z. Z. Lin and D. P. Tang, *Biosens. Bioelectron.*, 2017, **96**, 317–323.
13 X. Zhang, K. N. Chi, D. L. Li, Y. Deng, Y. C. Ma, Q. Q. Xu, R. Hu and Y. H. Yang, *Biosens. Bioelectron.*, 2019, **129**, 64–71.
14 H. X. Lu, G. Q. Wang, R. H. Dai, X. Ding, M. C. Liu, H. H. Sun, C. Q. Sun and G. H. Zhao, *Electrochim. Acta*, 2019, **324**, 134820.
15 X. Y. Jiang, L. Zhang, Y. L. Liu, X. D. Yu, Y. Y. Liang, P. Qu, W. W. Zhao, J. J. Xu and H. Y. Chen, *Biosens. Bioelectron.*, 2018, **107**, 230–236.
16 W. W. Zhao, J. J. Xu and H. Y. Chen, *Biosens. Bioelectron.*, 2017, **92**, 294–304.
17 L. Zhang, Y. L. Shen, G. C. Fan, M. Xiong, X. D. Yu and W. W. Zhao, *Microchim. Acta*, 2019, **186**, 284.
18 Y. T. Xu, S. Y. Yu, Y. C. Zhu, G. C. Fan, D. M. Han, P. Qu and W. W. Zhao, *TrAC, Trends Anal. Chem.*, 2019, **114**, 81–88.
19 B. D. Yan, Y. Zhuang, Y. L. Jiang, W. Xu, Y. J. Chen, J. C. Tu, X. H. Wang and Q. Wu, *Appl. Surf. Sci.*, 2018, **458**, 382–388.
20 L. H. He, Q. B. Liu, S. J. Zhang, X. T. Zhang, C. L. Gong, H. H. Shu, G. J. Wang, H. Liu, S. Wen and B. Q. Zhang, *Electrochem. Commun.*, 2018, **94**, 18–22.
21 L. Xia, J. Song, R. Xu, D. L. Liu, B. Dong, L. Xu and H. W. Song, *Biosens. Bioelectron.*, 2014, **59**, 350–357.
22 G. M. Ryu, M. Lee, D. S. Choi and C. B. Park, *J. Mater. Chem. B*, 2015, **3**, 4483–4486.
23 F. Y. Liu, P. Wang, Q. Q. Zhang, Z. Y. Wang, Y. Y. Liu, Z. K. Zheng, X. Y. Qin, X. Y. Zhang, Y. Dai and B. B. Huang, *Electroanalysis*, 2019, **31**, 1809–1814.
24 G. L. Wang, K. L. Liu, Y. M. Dong, X. M. Wu, Z. J. Li and C. Zhang, *Biosens. Bioelectron.*, 2014, **62**, 66–72.
25 X. Y. Zhang, F. Xu, B. Q. Zhao, X. Ji, Y. W. Yao, D. P. Wu, Z. Y. Gao and K. Jiang, *Electrochim. Acta*, 2014, **133**, 615–622.
26 H. B. Li, J. Li, Y. Y. Zhu, W. Y. Xie, R. Shao, X. X. Yao, A. Q. Gao and Y. D. Yin, *Anal. Chem.*, 2018, **90**, 5496–5502.
27 Y. Wang, L. Bai, Y. Wang, D. Qin, D. Shan and X. Lu, *Analyst*, 2018, **143**, 1699–1704.
28 S. Wu, H. Huang, M. Shang, C. Du, Y. Wu and W. Song, *Biosens. Bioelectron.*, 2017, **92**, 646–653.
29 M. X. Shang, H. Qi, C. C. Du, H. Huang, S. Y. Wu, J. L. Zhang and W. B. Song, *Sens. Actuators, B*, 2018, **266**, 71–79.
30 B. Peng, L. Tang, G. Zeng, S. Fang, X. Ouyang, B. Long, Y. Zhou, Y. Deng, Y. Liu and J. Wang, *Biosens. Bioelectron.*, 2018, **121**, 19–26.
31 X. Li, Y. J. Yuan, X. M. Pan, L. Z. Zhang and J. M. Gong, *Biosens. Bioelectron.*, 2019, **123**, 7–13.
32 H. H. Huo, Z. D. Xu, T. Zhang and C. L. Xu, *J. Mater. Chem. A*, 2015, **3**, 5882–5888.
33 P. P. Liu, X. Q. Liu, X. H. Huo, Y. F. Tang, J. Xu and H. X. Ju, *ACS Appl. Mater. Interfaces*, 2017, **9**, 27185–27192.
34 F. X. Wang, C. Ye, S. Mo, H. Q. Luo, J. R. Chen, Y. Shi and N. B. Li, *Anal. Bioanal. Chem.*, 2019, **411**, 3059–3068.
35 L. M. Guo, Z. Li, K. Marcus, S. Navarro, K. Liang, L. Zhou, P. D. Mani, S. J. Florczyk, K. R. Coffey, N. Orlovskaya, Y. H. Sohn and Y. Yang, *ACS Sens.*, 2017, **2**, 621–625.
36 T. Zhang, Y. Hou, V. Dzhagan, Z. Q. Liao, G. L. Chai, M. Loffler, D. Olianas, A. Milani, S. Q. Xu, M. Tommasini, D. R. T. Zahn, Z. K. Zheng, E. Zschech, R. Jordan and X. L. Feng, *Nat. Commun.*, 2018, **9**, 1140.
37 H. J. Sun, C. Neumann, T. Zhang, M. Loffler, A. Wolf, Y. Hou, A. Turchanin, J. Zhang and X. L. Feng, *Adv. Mater.*, 2019, **31**, 1900961.
38 H. J. Sun, I. H. Oner, T. Wang, T. Zhang, O. Selyshchev, C. Neumann, Y. B. Fu, Z. Q. Liao, S. Q. Xu, Y. Hou, A. Turchanin, D. R. T. Zahn, E. Zschech, I. M. Weidinger, J. Zhang and X. L. Feng, *Angew. Chem., Int. Ed.*, 2019, **58**, 10368–10374.
39 L. Wang, Y. Y. Wan, Y. J. Ding, S. K. Wu, Y. Zhang, X. L. Zhang, G. Q. Zhang, Y. J. Xiong, X. J. Wu, J. L. Yang and H. X. Xu, *Adv. Mater.*, 2017, **29**, 1702428.
40 H. B. Li, J. Li, D. Y. Chen, Y. X. Qiu and W. Wang, *Sens. Actuators, B*, 2015, **220**, 441–447.
41 S. Y. Yu, Y. Gao, F. Z. Chen, G. C. Fan, D. M. Han, C. S. Wang and W. W. Zhao, *Sens. Actuators, B*, 2019, **290**, 312–317.
42 W. X. Dai, L. Zhang, W. W. Zhao, X. D. Yu, J. J. Xu and H. Y. Chen, *Anal. Chem.*, 2017, **89**, 8070–8078.
43 L. Zhang, Y. F. Ruan, Y. Y. Liang, W. W. Zhao, X. D. Yu, J. J. Xu and H. Y. Cheng, *ACS Appl. Mater. Interfaces*, 2018, **10**, 3372–3379.
44 Y. H. Zhu, K. Yan, Z. W. Xu, J. N. Wu and J. D. Zhang, *Biosens. Bioelectron.*, 2019, **131**, 79–87.
45 X. M. Shi, C. D. Wang, Y. C. Zhu, W. W. Zhao, X. D. Yu, J. J. Xu and H. Y. Chen, *Anal. Chem.*, 2018, **90**, 9687–9690.
46 X. C. Wang, K. Maeda, A. Thomas, K. Takanabe, G. Xin, J. M. Carlsson, K. Domen and M. Antonietti, *Nat. Mater.*, 2009, **8**, 76–80.
47 J. K. Liu, S. H. Wen, Y. Hou, F. Zuo, G. J. O. Beran and P. Y. Feng, *Angew. Chem., Int. Ed.*, 2013, **52**, 3241–3245.
48 X. Y. Yang, Y. Gao, Z. P. Ji, L. B. Zhu, C. Yang, Y. Zhao, Y. Shu, D. Q. Jin, Q. Xu and W. W. Zhao, *Anal. Chem.*, 2019, **91**, 9356–9360.
49 R. Du, N. Zhang, H. Xu, N. N. Mao, W. J. Duan, J. Y. Wang, Q. C. Zhao, Z. F. Liu and J. Zhang, *Adv. Mater.*, 2014, **26**, 8053–8058.
50 J. Y. Zhou, X. Gao, R. Liu, Z. Q. Xie, J. Yang, S. Q. Zhang, G. M. Zhang, H. B. Liu, Y. L. Li, J. Zhang and Z. F. Liu, *J. Am. Chem. Soc.*, 2015, **137**, 7596–7599.
51 P. P. Liu, X. H. Huo, Y. F. Tang, J. Xu, X. Q. Liu and D. K. Y. Wong, *Anal. Chim. Acta*, 2017, **984**, 86–95.
52 S. Ghosh, A. Priyam, S. C. Bhattacharya and A. Saha, *J. Fluoresc.*, 2009, **19**, 723–731.
53 D. A. Armstrong, R. E. Huie, W. H. Koppenol, S. V. Lymar, G. Merenyi, P. Neta, B. Ruscic, D. M. Stanbury, S. Steenken and P. Wardman, *Pure Appl. Chem.*, 2015, **87**, 1139–1150.
54 P. M. Wood, *Biochem. J.*, 1988, **253**, 287–289.

